

Microchannel plate electro-osmotic pump

Z. Cao · L. Yuan · Y.-F. Liu · S. Yao ·
L. Yobas

Received: 16 December 2011 / Accepted: 22 February 2012 / Published online: 6 March 2012
© Springer-Verlag 2012

Abstract Microchannel plate (MCP), a porous glass membrane commonly used as an electron multiplier in particle detectors, has been experimentally investigated here for electro-osmotic pumping characteristics. MCP consists of millions of high-aspect ratio precision identical glass microcapillary tubes fused together. Uniform and straight microchannels in a relatively thick membrane can achieve a maximum flow rate per unit area and voltage $\sim 0.2 \text{ mL min}^{-1} \text{ cm}^{-2} \text{ V}^{-1}$ and a maximum pressure per unit voltage $\sim 80 \text{ Pa V}^{-1}$. MCP also shows a unique characteristic of directional preference in pumping with net flow consistently induced toward the nearest electrode regardless of polarity of the voltage potential applied.

Keywords Microchannel plate (MCP) · Microchannels · Pump · Electro-osmosis (EO) · Induced-charge electrokinetic (ICEK)

1 Introduction

With a simplistic structure and no moving part, electro-osmotic (EO) pumps attract a great deal of attention from a

broad spectrum of fields including electronic cooling (Jiang et al. 2002), drug delivery (Chen et al. 2007), mechanical actuation (Prakash et al. 2006), capillary-column liquid chromatography (Chen et al. 2004), flow-injection analysis (Liu and Dasgupta 1992), and lab on a chip (Brask et al. 2005). Unlike mechanical pumps, EO pumps are compact, easy to integrate and operate, and can generate a non-pulsating flow (Wang et al. 2009; Laser and Santiago 2004). Among all, they scale favorably with microfluidics and can be made through a variety of techniques.

EO pumps operate based on the principle of electro-osmosis, the phenomenon identified with the bulk liquid flow as a result of an applied electric field tangential to a surface (e.g. capillary wall). Most surfaces that are brought in contact with a polar liquid are known to acquire a net charge spontaneously through electrochemical reactions (Hunter 1981). The net surface charge causes redistribution of the nearby ions in liquid by attracting counter-ions, while repelling co-ions. This ionic redistribution leads to an electrical double layer (EDL) with a compact inner layer of counter-ions (Stern layer) that are stagnant near the surface and a diffused outer layer of counter-ions (Gouy–Chapman layer) that are mobile. The mobile counter-ions can move under the Coulomb force of an applied electric field and drag along the bulk liquid through viscous coupling. This electro-osmotic flow expresses a uniform plug-like velocity profile (except very near the walls), in contrast with the parabolic velocity profile of a pressure-driven flow.

EO pumps, thus far, can be categorized according to their morphology as open-channel, packed-column, porous-monolith, and porous-membrane pumps. The open-channel type can be as simple as a single capillary tube (Dasgupta and Liu 1994) or a planar substrate with lithographically structured microchannels (Lazar and Karger 2002). The latter has the added advantage of microfluidic

Z. Cao and L. Yuan contributed equally.

Z. Cao · L. Yuan · Y.-F. Liu · L. Yobas (✉)
Department of Electronic and Computer Engineering,
Hong Kong University of Science and Technology,
Clear Water Bay, Kowloon, Hong Kong SAR, China
e-mail: eelyobas@ust.hk

S. Yao
Department of Mechanical Engineering, The Hong Kong
University of Science and Technology, Clear Water Bay,
Kowloon, Hong Kong SAR, China

integration with miniaturized components on the same chip. The open-channel type is capable of delivering impressive flow rates and yet against low backpressures. This is mainly due to the limited surface area-to-volume ratio (SVR) of quasi two-dimensional microchannels. Meanwhile, the packed-column type, trading off the flow rate, increases the SVR, and thus the pressure output considerably (Paul et al. 1998; Chen et al. 2003). However, this type requires dense packing of beads between frits. Reproducible and void-free fabrication of the frits as well as packing of the beads can be problematic, especially given that they have to endure large forces exerted by the high-pressure output. The frits can be replaced by in situ weir microstructures etched lithographically (Razunguzwa and Timperman 2004; Borowsky et al. 2008). The porous-monolith type also eliminates the need for frits by replacing the packed beads with a porous monolith, which can be of an organic polymer or inorganic silica, fixed in the column through polymerization (Zou et al. 2002; Tanaka et al. 2002; Tripp et al. 2004). During polymerization, however, shrinking monolith could lead to too many voids for the pump to be able to maintain a stable flow rate. A common aspect in all the articulated pump types is the requirement of high voltages due to a relatively large electrode gap imposed by the high-aspect ratio channels or columns. Exempted from this requirement is the porous-membrane type which allows the gap to be reduced by directly integrating the electrodes on the opposing surfaces of the pump membrane (Miao et al. 2007). This type also retains a large SVR as the entire membrane is penetrated with pores. The pores, however, in a membrane of typically a sintered glass powder (Gan et al. 2000; Yao et al. 2003) or a polymerized monolith (Tripp et al. 2004) exhibit a broad size distribution and tortuous random paths, a characteristic that degrades the overall flow rate.

Recently, the interest in low-voltage high flow-rate applications has motivated the development of membrane-type EO pumps with orderly aligned, nearly cylindrical channels having straight walls (tortuosity approaching unity). Such pumps have already been demonstrated in porous-silicon (Yao et al. 2006; Wallner et al. 2007) and porous-aluminum oxide membranes (Miao et al. 2007; Vajandar et al. 2007; Ai et al. 2010; Prakash et al. 2006). Both the membrane materials can be porosified via electrochemical etching (anodization) after their pore locations being marked via the lithographic patterning. Yao et al. (2006) fabricated porous-silicon membranes, each with dimensions 1 cm × 1 cm and a thickness 350 μm. Based on the pore diameter (2–6 μm), the measured flow rates and pressures for a sodium borate buffer (1 mM) can reach up to 16 mL min⁻¹ and 70 kPa with the applied voltages <100 V. Similarly, Wallner et al. (2007) investigated macroporous silicon membranes with a diameter 3.5 mm

and a thickness >500 μm. Having pores at a diameter 3.6 μm and a density of 5.4 × 10⁶ cm⁻², the pump can supply maximum ~85 μL min⁻¹ or 5.2 kPa de-ionized (DI) water at 60 V. Miao et al. (2007) fabricated anodic aluminum oxide (AAO) membranes with unspecified dimensions and a thickness in the range 20–75 μm. The AAO membranes, through proper annealing and chemical treatments followed by silica coating, can achieve significantly increased flow rates (DI water) 86 mL min⁻¹ cm⁻² at 70 V. Xu et al. (2011) modified the porosification process for silicon membranes by replacing the anodization step with deep reactive ion etching (DRIE). The membranes with an active area ~3 mm² and a thickness 50 μm contained 3.5 μm-diameter pores at a pitch 7.7 μm. The pump can deliver DI water at an impressive flow rate of ~200 mL min⁻¹ cm⁻² with a 30 V direct current (DC) actuation. The authors also demonstrated a digital actuation scheme in which the pump output can be controlled by the duty cycle of voltage pulses. This actuation scheme reportedly resolved the issues with the flow regulation and stability.

Here, we introduce a novel porous media for the membrane-type EO pumps with microfabrication and morphology, distinctively unique from those reported so far. This membrane, also known as the microchannel plate (MCP), serves as an electron multiplier in many particle and photon detectors (Wiza 1979). MCP is a compact glass-based membrane housing millions of closely packed identical cylindrical microcapillaries (Fig. 1). It is manufactured by various suppliers through glass fiber drawing process borrowed from the fiber-optic technology. Inherent to the fiber drawing process is a high degree of dimensional uniformity from channel to channel, a feature desired in an EO pump. Achieving such high-aspect ratio straight-wall channels through lithography-based methods (e.g., reactive ion etching or electrochemical anodization) can be challenging as it either burdens the etch process or may not lead to ideal porosity due to incompletely formed channels. Thus, we are motivated to investigate the novel use of this membrane as an EO pump and report here our preliminary results.

2 Methods

2.1 MCP

The MCPs characterized in this study were purchased from Chairman Photoelectricity S&T Co. Ltd, P. R. China. Figure 1 depicts the scanning electron microscopy images of a cross-sectioned MCP. As seen, it offers an ideal morphology for electro-osmotic pumping. It contains a highly regular array of microcapillaries each 5 μm in diameter over a large span (diameter 18 mm). This porous

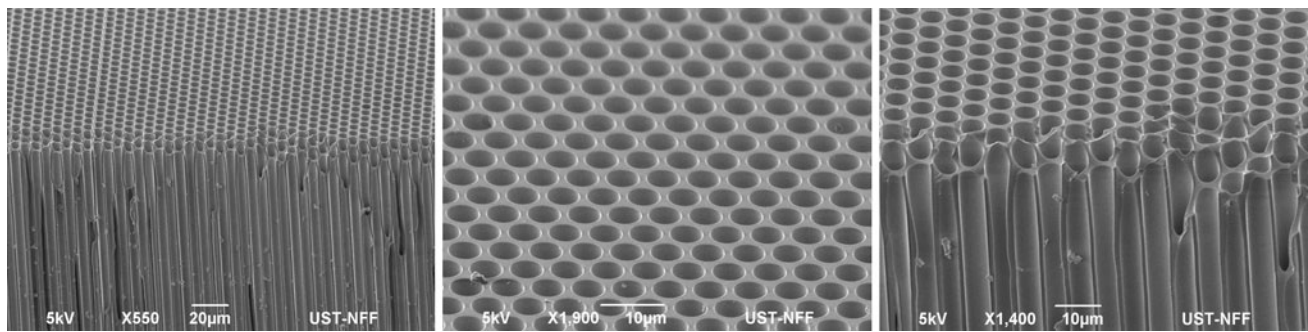


Fig. 1 Scanning electron microscopy images of a cross-sectioned MCP revealing highly regular, densely packed, and high-aspect ratio (1:60) microchannels 5 μm in diameter with smooth and straight

sidewalls. Note that the *sidewalls* appear *slightly curved* due to the randomness of the sectioning angle

region densely packs millions of ($\sim 12 \times 10^6$) microcapillaries ($4.7 \times 10^6 \text{ cm}^{-2}$). Thus, the porosity 0.93 is much larger than the pump media reported so far. In addition, the glass microcapillaries possess very large aspect ratio ($\sim 1:60$) with straight and smooth sidewalls running through a membrane that is about 300 μm thick. The manufacturing process of the MCP greatly deviates from those of the known pump media. The process is schematically illustrated in Fig. 2. Briefly, it involves a series of fiber draws (Wiza 1979). The first draw produces a glass monofiber (diameter $\sim 1 \text{ mm}$) with an acid-soluble sacrificial core and an alkali-soluble lead glass cladding which forms the MCP matrix structure. Identical monofibers are stacked together in a hexagonal array to obtain a perform (first stack) for the subsequent draw. This second draw produces the basic building block of the MCP, known as the multifiber. The multifibers are stacked again (second stack) and fused within a glass envelope to form a boule under high-temperature vacuum. The boule is turned into thin plates with desired thickness and shape by following the standard semiconductor slicing, lapping, and polishing techniques. The plates are then chemically etched to remove the soluble solid glass core from all the monofibers, thereby forming the microcapillaries. To achieve a semi-conducting surface with a desired secondary electron yield suitable for an electron multiplier, the lead glass is reduced by firing the plates in hydrogen furnace. Thin-film metal electrodes are placed on both sides of the plates during manufacturing to ensure that the same potential is applied to each microcapillary. The MCPs are also offered without a thin-film surface metal and those characterized here did not go through the electrode evaporation step.

2.2 Pump assembly

The MCP was mounted on a structured acrylic frame ($\sim 1 \text{ mm}$ thick) and secured in place by a silicone adhesive (Fig. 3a). The adhesive was separated from the pores by a

2 mm solid glass border surrounding the porous region (opaque area). The frame with the MCP was then assembled in a custom-made housing for electrical and fluidic connections. The pump housing included a pair of polycarbonate containers (Fig. 3b). Both the containers were sealed on their sides with an acrylic cover plate to allow sighting of the MCP and the electrodes (Fig. 3c). Either electrode was prepared by weaving a mesh of a platinum wire 0.25 mm in diameter across a copper flange (1 mm thick). These were then assembled according to their respective order and clamped together by passing metal rods through them. The metal rods had an insulating sleeve around them to guard against shorting the electrodes. The electrodes were separated by a nominal distance of 3 mm as dictated by the thickness of the respective copper flanges and of the acrylic frame. External wires were directly soldered on the copper flanges, while plastic tubes were connected to the fluidic fittings built into the polycarbonate containers (Fig. 3b).

2.3 Experimental setup

The MCPs, as soon as unpacked, were assembled in the pump housing. The pump and the tubings were then filled with DI water carefully and visually inspected to ensure that no air bubbles were trapped. Conductivity of the pump liquid, DI water, was measured before and after the experiments (Mettler Toledo). To activate the pump, a direct-current (DC) voltage was applied in the range of 0–100 V to the electrodes from a high-voltage power supply (HP, 6035A). Figure 4 shows a schematic of the test setup for the measurement of the pump characteristics as a function of the DC voltage applied. For an applied voltage, pressure capacity was measured by recording the maximum achievable differential height between the water menisci of the pump inlet and the outlet tubes. Flow capacity was measured against a zero differential water column by sampling and weighing the water output of the pump on a precision balance (Sartorius, BSA224S) at fixed

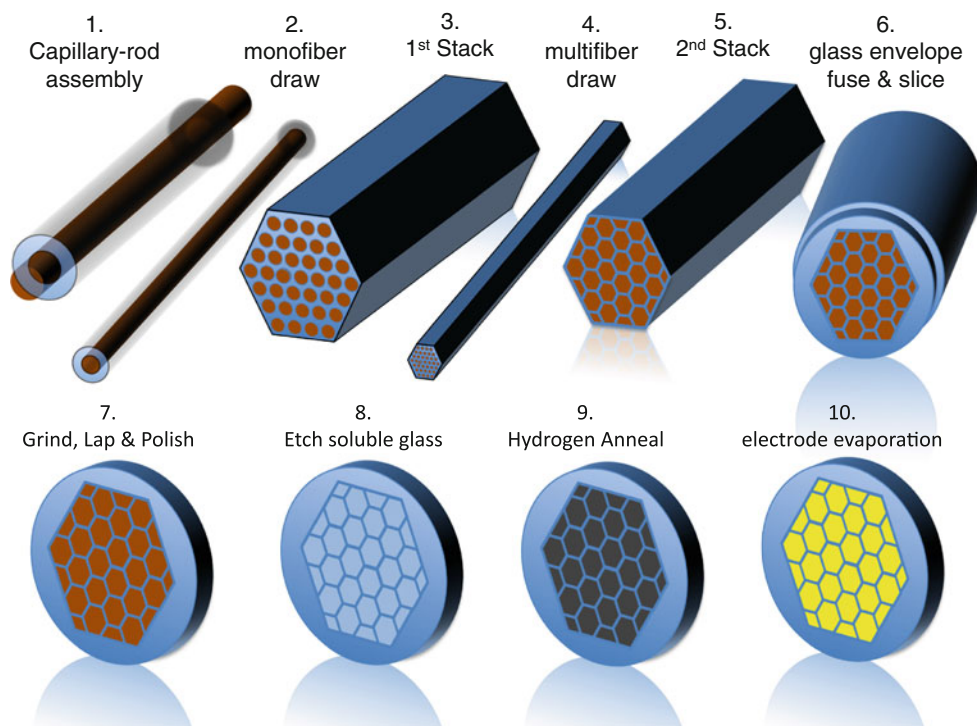


Fig. 2 Key process steps involved in the microfabrication of MCP (the samples tested here did not go through the last step of electrode evaporation)

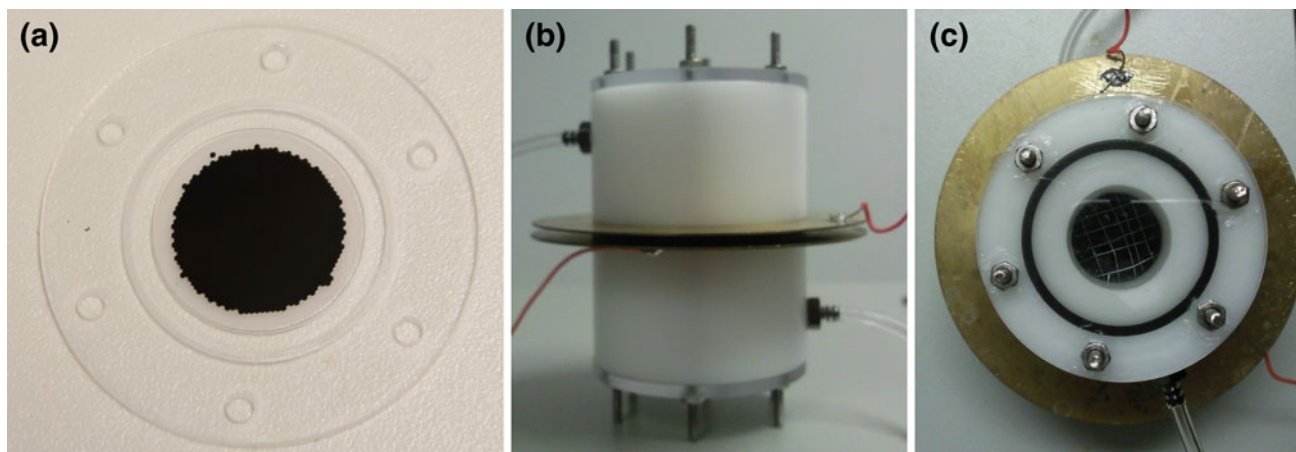


Fig. 3 Pictures of **a** the MCP as mounted on an acrylic frame before being assembled into the pump housing shown from **b** side, and **c** above. The opaque area surrounded by the solid glass border is the

porous region of the MCP. The MCP as well as the platinum mesh electrode can be partially seen through the acrylic window (c)

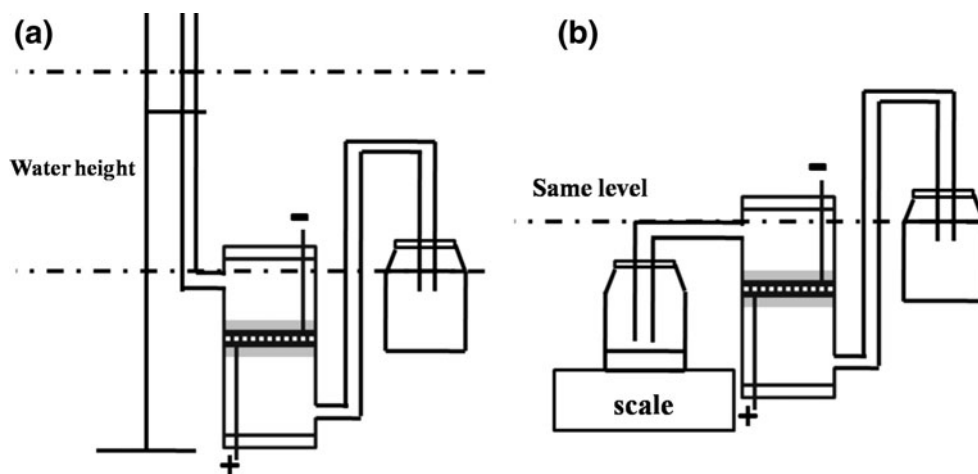
time intervals. Alternatively, flow capacity was also measured by tracking the meniscus position within the outlet tube over time, while maintaining a zero differential water column.

3 Results and discussion

The EO pump characteristics were investigated on two identical MCPs. Figure 5 shows the plots of the pump

characteristics including maximum flow rate (Q_{\max}), maximum current (I_{\max}), and maximum pressure (P_{\max}), all as a function of the effective voltage across the MCPs (V_{eff}). By definition, Q_{\max} and I_{\max} refer to the measurements against zero backpressure whereas P_{\max} is measured at a zero net flow rate. While the applied voltage across the electrodes (V_{app}) varies up to 100 V DC, only a small fraction of this voltage (<10 V) predictably appears across the MCP after the losses due to decomposition potential of

Fig. 4 Schematics of the experimental setup (not drawn to scale) employed to measure the pump characteristics as a function of DC voltage applied: **a** maximum pressure at zero net flow rate; **b** maximum flow rate against zero backpressure



the electrodes (V_{dec}) and their voltage dividing separation. Thus, V_{eff} can be stated as:

$$V_{eff} = r(V_{app} - V_{dec}) \tag{1}$$

where r is the ratio of the resistance through the MCP to the equivalent resistance of all the three sections in series, including the MCP and the electrolyte-filled gaps between the MCP and the either electrode. V_{dec} is due to the electrode reactions at the electrode/electrolyte interface and approximated by the electrode overpotential. V_{dec} and r can be empirically determined from the current–voltage plot of the pump assembly, wherein the MCP is excluded: V_{dec} refers to the x -intercept while r being the slope multiplied by the resistance through the MCP. Accordingly, V_{dec} and r were evaluated here as 2.34 V and 0.11, respectively.

As shown in Fig. 5, both MCPs exhibit a linear trend in their pump characteristics of Q_{max} , I_{max} , and P_{max} with the effective voltage V_{eff} (Note R^2 values). Slight deviations observed between the two pumps appear to be within the error of measurements, although those pertaining to Q_{max} and I_{max} tend to grow with the voltage applied. A major contributor to the observed discrepancy could be the electrolytic gas bubbles formed during the pumping. Evolved gas bubbles were observed on the electrodes particularly at higher voltages. These bubbles possibly impede the fluidic and ionic flow through the pump causing the deviations shown in Fig. 5a, b. Unlike, the measurements of maximum pressure capacity between the two pumps are quite consistent probably because of the recirculating nature of flow in this regime, which could clear off the bubbles from the electrodes. To mitigate electrolytic gas bubbles, researchers introduced various remedies such as the inclusion of a gas recombination unit (Yao et al. 2003), the utilization of special electrodes (Ag/Ag₂O) consumed in the pumping process (Shin et al. 2011), or a periodic current waveform with zero net charge and yet non-zero potential drop between the electrodes

(Selvaganapathy et al. 2002). Despite the bubbles, the highest flow rate measured per unit effective voltage and per unit area (the total pore area 2.36 cm²) is around 0.2 mL min⁻¹ cm⁻² V⁻¹ which is about seven times larger than the silica-based frit pumps (Yao et al. 2003) and comparable to the value reported for porous-silicon membrane pumps of similar dimensions (Yao et al. 2006).

The MCP, owing to its highly parallel well-defined microchannels, can be modeled as a bundle of identical straight-wall cylindrical capillaries. Following the theoretical analysis of Rice and Whitehead (1965), for an electro-osmotic flow in a cylindrical capillary and assuming a thin EDL limit (microchannels 5 μm in diameter vs. the Debye length ~100 nm, the characteristic dimension of EDL in DI water), we can simply put P_{max} and Q_{max} per unit voltage V_{eff} as (Laser and Santiago 2004; Reichmuth et al. 2003):

$$\frac{P_{max}}{V_{eff}} = -\frac{8\varepsilon\zeta}{a^2} \quad \frac{Q_{max}}{V_{eff}} = -\frac{n\pi a^2\varepsilon\zeta}{\mu L} \tag{2}$$

where ε and μ are the permittivity ($\sim 7 \times 10^{-10}$ F m⁻¹) and the viscosity (1×10^{-3} Pa s) of the liquid pumped (DI water), respectively; ζ is the zeta potential; a is the radius of the microchannels (2.5 μm); n is the population of the microchannels (12×10^6); L is the length of the microchannels limited by the thickness of the MCP (300 μm).

For a uniform ζ potential, maximum pressure and maximum flow rate per unit effective voltage remain constant. This is based on the assumption that permittivity and viscosity of the liquid do not considerably vary over time during the measurements. Either ratio in (1) refers to the slope of the respective plot in Fig. 5 and can be employed to evaluate ζ potential of the MCP under test. As the main use of the MCP is in the area of imaging, the value of ζ potential is not readily available. The highest measured pressure per unit effective voltage is ~ 80 Pa V⁻¹ and suggests a value for ζ potential,

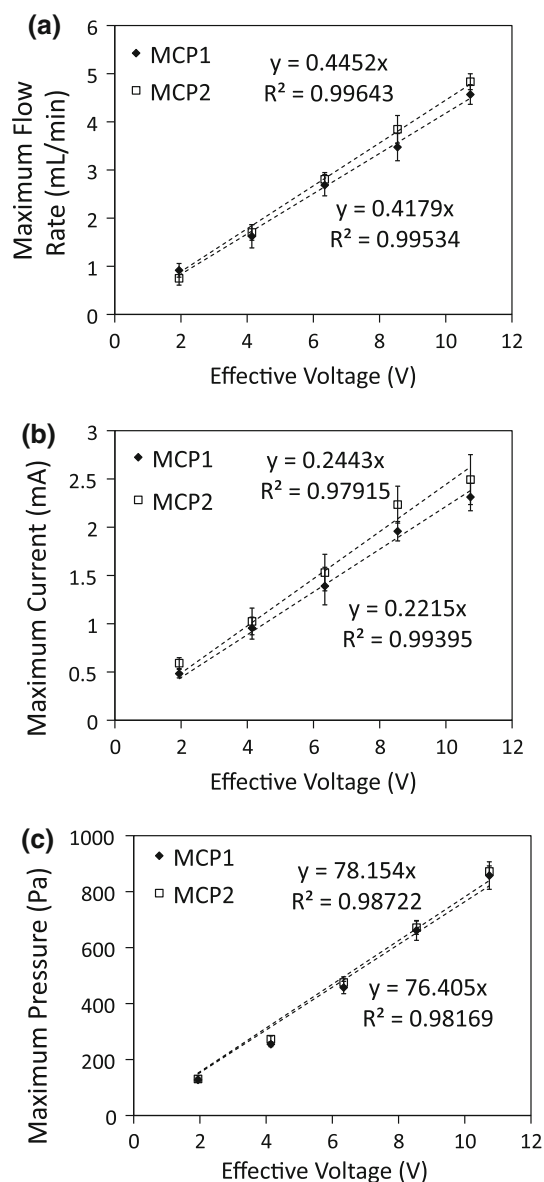


Fig. 5 Measured pump characteristics of two identical MCPs **a** maximum flow rate, **b** maximum current, and **c** maximum pressure as a function of effective voltage. Symbols and error bars represent the mean and \pm standard deviation values of repeat measurements (six repeats for each data point), respectively. The two MCPs have the same structure: pore diameter $5 \mu\text{m}$, pore density $4.7 \times 10^6 \text{cm}^{-2}$ and membrane thickness $300 \mu\text{m}$

approximately -90 mV more or less comparable to those reported for glass. Meanwhile the highest measured flow rate per unit effective voltage is $\sim 0.5 \text{ mL min}^{-1} \text{ V}^{-1}$ and implies relatively low values for ζ potential of -15 mV . Such disagreement can also be found in earlier reports. For instance, Yao et al. (2006) showed that a typical value of ζ potential -104 mV measured for porous-silicon membranes with an oxide surface provides a reasonable prediction of the highest flow rate measurements, while it can overestimate the measured pressure capacity by up to 85%

depending on the pore size. Although their trend is opposite of ours (overestimated flow capacity), the authors attribute their uncertainty to several factors including possible drop in local pH and zeta potential at low flow rates (during the measurement of maximum pressure capacity), non-uniform pores, and inaccurate pore size. Consistent with the trend here, Wallner et al. (2007) independently demonstrated for macroporous silicon that a ζ potential value of -50.58 mV fits well with the pressure capacity measurements, but it overestimates the measured flow capacity by several orders of magnitude. The authors attribute such unusually low flow capacity to fluidic resistance of their experimental setup. This inconsistency will be further iterated below.

Alternatively, one can evaluate ζ potential from the ratio of maximum flow rate to maximum current, both measured simultaneously against a zero backpressure (Yao et al. 2003):

$$\frac{Q_{\max}}{I_{\max}} = -\frac{\varepsilon\zeta}{\mu\sigma} \quad (3)$$

where σ is the ionic conductivity of the liquid (DI water) measured here before and after experiments: $\sim 1 \mu\text{S cm}^{-1}$ and $\sim 5 \mu\text{S cm}^{-1}$, respectively. As can be noticed, during the experiments, the ionic conductivity of the DI water increases considerably. This increase is not unexpected, given that the handling of DI water is known to increase its conductivity, while reducing its pH slightly, possibly due to the adsorption of atmospheric carbon dioxide (Zeng et al. 2001).

In our experiments, the ratio of maximum flow rate to maximum current is $\sim 2 \text{ mL min}^{-1} \text{ mA}^{-1}$ as can be deduced from the ratio of the respective slopes in Fig. 5. This suggests ζ potential of -25 mV for a conductivity of $5 \mu\text{S cm}^{-1}$, while -100 mV for $20 \mu\text{S cm}^{-1}$. The former value is comparable to ζ potential obtained from the measurements of highest flow rate, whereas the latter is closer to the value suggested by the measurements of highest pressure. Yet, the former is based on a conductivity value more representative of the readings at the conclusion of the experiments. Hence, the value of -15 mV seems more plausible for ζ potential of the MCP.

The pump capacity for generating a reasonable flux of liquid against a downstream backpressure is critical for practical use of the pump and was also investigated. The backpressure across the pump was maintained at a set-value by raising the output column to the required height and harvesting the freshly pumped liquid from the tube outlet at that height. The liquid output was collected for a fixed period of time and then weighed to calculate the flow rate. All measurements were performed at $V_{\text{eff}} = 8.5 \text{ V}$, a plot of the measured values is shown in Fig. 6. The flow rate, as expected, declines inversely with the backpressure following a linear fitting. Considering a typical operating

point in the middle of the plot, a conservative estimate of the pump efficiency η can be calculated as 0.039% by substituting current 2 mA, effective voltage 8.5 V, maximum pressure 400 Pa, and maximum flow rate 4 mL min⁻¹ in (4).

$$\eta = \frac{1}{4} \frac{P_{\max} Q_{\max}}{V_{\text{eff}} I} \tag{4}$$

In the measurements reported above, the pumping direction was observed toward the cathode (negatively charged electrode), same as the flow direction for most glass membrane pumps, and with the flow rate reaching steady state within a second. However, when the voltage polarity was reversed, the pumping direction did not change. It was noticed that the MCP consistently pumps the liquid toward a particular direction, irrespective of the polarity of the DC voltage applied across the electrodes. This directional preference so far has not been reported for the known porous-membrane pumps as their surface typically expresses a fixed value for ζ potential that is mostly negative for the majority of glass types (due to deprotonation of acidic silanol groups). Thus, the net electro-osmotic flow is normally established by counter-ions (cations) drifting toward the cathode and reverses its direction in response to a change in the polarity of the DC voltage being applied.

Further examination of the pump assembly suggested that the direction of pumping appears toward the electrode situated nearest to the MCP. In the pump, the MCP sits slightly closer to a particular electrode (by about 1 mm) due to asymmetric profile of the acrylic frame structure in which it is mounted. This hypothesis was validated by a simple test where the MCP is specifically distanced from the favored electrode by introducing a thin spacer layer (~1 mm thick) in the assembly and thereby bringing it nearer to the opposite electrode. In return, the pumping direction reversed for the same polarity of the DC voltage applied, prior to the inclusion of the spacer.

To enhance the surface ζ potential and influence the pumping direction (to maintain always toward the cathode

as in other glass membranes), two separate surface treatment methods have been independently experimented on the same MCP. In the first method, the MCP was incubated in ammonia solution (29 wt% NH₄OH:30 wt% H₂O₂:DI water) overnight and then measured for its pump characteristics whereas, in the second method, the MCP, once it recovered from the first treatment, was exposed to oxygen plasma briefly (<10 min) and then measured again. Either method is known to generate hydrophilic channel walls by introducing surface hydroxyl (silanol) groups albeit lasting only for a short while (Gale et al. 2008; Bhattacharya et al. 2005). These groups ionize (deprotonate) in solution and impart a net negative charge on the surface. Ammonia also slightly etches glass regenerating its surface. Through either method, a change was noticed in the pump behavior: the MCP began to pump consistently toward the cathode as commonly observed with the glass membranes reported. Switching the polarity of the applied voltage also caused a reversal in the pumping direction. Figure 7 shows the highest pressure measured as a function of effective voltage upon either treatment in several repeat measurements taken consecutively. Apart from the pumping direction, no dramatic change in the highest pressure capacity was observed. As can be noticed, the pump performance degrades with each successive series of measurements, suggesting that the surface state attained by either treatment method was temporary. In fact, the MCP regained its original behavior after a while and began to pump toward the nearest electrode. That prevented further characterization of the new surface state for maximum flow rate and maximum current.

It is not clear at this moment the exact mechanism responsible for the observed unique pumping characteristic of the MCP; the induced flow toward the nearest electrode regardless of the polarity of the DC potential applied. Besides the classical electro-osmotic flow, additional mechanisms appear to be at play in physical and/or chemical origin unlike the other silica-based porous membranes. This might further explain the disagreements in the values of ζ potential obtained with the measurements subjected to the above equations that consider electro-osmosis alone. Several likely candidates to elucidate the observed behavior are worthy of consideration including induced pressure gradient, nonlinear electrokinetic effects, and faradaic reactions. Induced pressure gradients develop to counterbalance any mismatch in electro-osmotic flow rates due to axial variations in ζ potential (Herr et al. 2000) and/or surface conductance (Yanagisawa and Dutta 2010) along a pore segment. Excess conduction that takes place in EDL also acts as a “short-circuit” reducing the applied electric field in the interface and the subsequent electro-osmotic flow (Jiménez et al. 2007; Xu et al. 2011; Lyklema and Minor 1998).

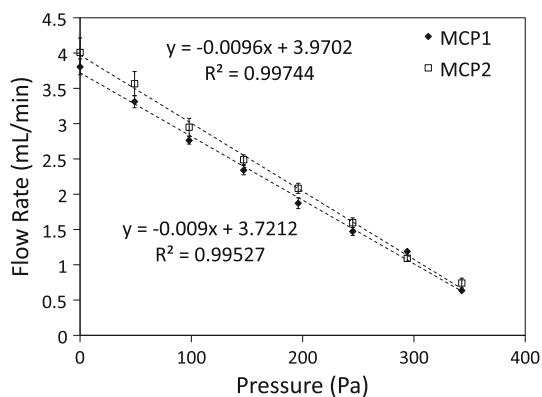


Fig. 6 Pump pressure versus flow rate measured at $V_{\text{eff}} = 8.5\text{V}$

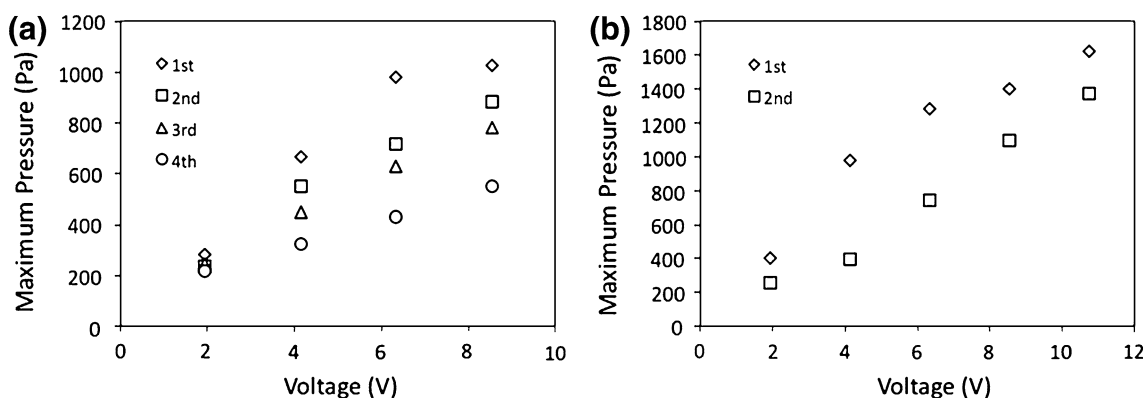


Fig. 7 Pump characteristics measured immediately after **a** the overnight incubation of the MCP in ammonia solution and then after, **b** the exposure to oxygen-plasma for 7 min. MCP pumps DI water toward

the negative electrode. *Symbols* refer to a different set of repeat measurements taken consecutively (the legends indicate their order). The pump capacity degrades with each consecutive measurement

Nonlinear induced-charge electrokinetic effects are observed around polarizable surfaces such as conductors, where an applied field acts upon the EDL that it has induced (Squires 2009). The MCP, although its bulk structure, is typically made of a lead silicate glass and does not qualify as a conductor, attains a semiconducting lead surface after the lead is reduced on the surface in hydrogen anneal (Wiza 1979). If the anneal is performed at too-high temperatures, the lead particles tend to form agglomerates on the surface. The presence of lead on the surface may cause a considerable shift in the steady ζ potential of silica (apart from the induced ζ) and possibly a non-uniform ζ across the surface because of the agglomerates (that leads to a pressure buildup). The induced EDL is superimposed over the steady equilibrium EDL and generally shows a dipolar arrangement, with positive ions on the side nearest the field source and negative ions on the side nearest the field sink. This charge arrangement is dynamic and reverses with the polarity of the applied voltage which might explain why the MCP does not reverse its pumping direction with the polarity of the applied DC voltage. To further check this hypothesis, an AC waveform was applied across the electrodes sweeping the frequency and magnitude over a broad range (10 Hz–100 kHz and 0–200 V_p). Nevertheless, this has failed to produce any noticeable net flow in any particular direction suggesting that an induced double layer, which is known to persist in AC fields, may not be a key player.

Lastly, faradaic reactions are considered given the semiconducting nature of the microcapillaries surface here. These electron-transfer reactions generate surface-normal currents that can perturb local surface potentials, ion concentrations, and thereby the equilibrium structure of EDL. This directly influences the electro-osmotic flow. Qian and Duval (2006) numerically modeled such flow through a conducting microcapillary subjected to an electric field and without any direct electrical contact with a power supply.

The authors employed the standard Butler–Volmer equation for the bipolar faradaic reactions taking place toward the opposing ends of the microcapillary. They showed that the spatial distributions of the electric field and ζ potential along the microcapillary could become highly nonlinear for an applied large field. Inevitably, this could induce a pressure gradient along the microcapillary that can drive flow together with complex electrostatic interactions between the nonlinear electric field and nonuniform ζ . Such configuration of an electrically floating conductor (or semiconductor) in contact with an ionic phase subjected to an electric field also applies to bipolar electrodes. Bipolar electrodes and faradaic reactions around them have been recently leveraged to concentrate, separate, and detect analytes in microfluidics (Mavré et al. 2010). The possibility of faradaic reactions taking place on the MCP became more evident, while characterizing the pump with an ionic solution, sodium borate buffer ($\text{Na}_2\text{B}_4\text{O}_7$) whereby extensive generation of gas bubbles were observed such that their accumulation on either side of the membrane caused a pressure build up, driving up the liquid columns. This occurred despite the low ionic concentration (1 mM) and low voltages (<10 V) which did not induce such effect on porous-silicon membranes (Yao et al. 2006).

As revealed here, MCP distinctively differs from the reported porous membranes not only in structure, but also in electrokinetic pumping characteristics (mechanism). Its distinctive microfabrication process involving several steps of fiber bundle drawing and sacrificial etching (the core glass versus the cladding glass) returns a high-porosity membrane with well-defined high-aspect ratio cylindrical microcapillaries. Alternative methods that can deliver such a structure are usually based on lithography and demand a highly controlled etching process to attain vertical and smooth sidewalls (since no sacrificial material is involved). DRIE microcapillaries with a similar aspect ratio take a considerable machine time and yields non-ideal sidewalls

(scallop). Electrochemical anodization usually fails to deliver all the pores completely formed leading to a reduced porosity. A fair comparison of the pump characteristics to those previously demonstrated is complicated by large variations in pump geometries and the way activation voltages reported (applied vs. effective). Nevertheless, the large pore size here, although it is the smallest we could get commercially, exceeds the range sought in membrane pumps and hence leads to the weak pressure capacity measured. The pore size could be reduced by coating a thin-film silica liner on the microcapillary walls through a surface sol-gel synthesis or an alternative deposition method (Toh et al. 2010; Vajandar et al. 2007; Miao et al. 2007). In addition to reducing the pore size, such coating on the microcapillary walls could help suppress the observed nonlinear behavior and improve the existing native ζ potential, which, as of now, may not deviate too much from that of silica, reportedly exhibiting two isoelectric points at pH 7 and 11 in the presence of lead ions (Rashchi et al. 1998).

4 Conclusions

MCP, a readily available porous-glass membrane used in image intensifier units as an electron multiplier, has been introduced here as an electro-osmotic pump. The pump characteristics were experimentally derived using DI water as the working liquid. MCP, with a highly ordered precision matrix (a bundle of tightly arranged straight-wall microchannels) can pump at a maximum capacity $\sim 80 \text{ Pa V}^{-1}$ (zero net flow) and $\sim 0.5 \text{ mL min}^{-1} \text{ V}^{-1}$ (against zero backpressure), for an effective voltage up to 11 V. We believe that the pump characteristics can be enhanced considerably and the ideal matrix structure can be leveraged fully by sparing MCP from this last step of hydrogen anneal. In return, this may also restore the normal behavior of a traditional EO pump; reversal of the flow direction with the polarity of the voltage applied. MCP can be used either as a stand-alone pump or embedded in microfluidic systems, after being segmented in smaller membranes. Thus, MCP can take away the burden of etching straight-wall precise microchannels from EO pump membranes.

Acknowledgments This project was financially supported in part by the Startup Grant from the ECE Department, HKUST, the Research Project Competition Grant by the HKUST (Grant No. RPC11EG09) and the Research Grant Council of Hong Kong, a Direct Allocation Grant to HKUST (Grant No. DAG09/10.EG09).

References

Ai Y, Yalcin SE, Gu D, Baysal O, Baumgart H, Qian S, Beskok A (2010) A low-voltage nano-porous electroosmotic pump. *J Colloid Interface Sci* 350(2):465–470

- Bhattacharya S, Datta A, Berg JM, Gangopadhyay S (2005) Studies on surface wettability of poly(dimethyl)siloxane (PDMS) and glass under oxygen-plasma treatment and correlation with bond strength. *J Microelectromech Syst* 14(3):590–597
- Borowsky JF, Giordano BC, Lu Q, Terray A, Collins GE (2008) Electroosmotic flow-based pump for liquid chromatography on a planar microchip. *Anal Chem* 80(21):8287–8292
- Brask A, Kutter JP, Bruus H (2005) Long-term stable electroosmotic pump with ion exchange membranes. *Lab Chip* 5(7):730–738
- Chen L, Ma J, Tan F, Guan Y (2003) Generating high-pressure sub-microliter flow rate in packed microchannel by electroosmotic force: potential application in microfluidic systems. *Sens Actuat B Chem* 88(3):260–265
- Chen LX, Ma JP, Guan YF (2004) Study of an electroosmotic pump for liquid delivery and its application in capillary column liquid chromatography. *J Chromatogr A* 2:219–226
- Chen LX, Choo J, Yan B (2007) The microfabricated electrokinetic pump: a potential promising drug delivery technique. *Expert Opin Drug Deliv* 4(2):119–129
- Dasgupta PK, Liu S (1994) Electroosmosis: a reliable fluid propulsion system for flow injection analysis. *Anal Chem* 66(11):1792–1798
- Gale GW, Small RJ, Reinhardt KA (2008) Aqueous cleaning and surface conditioning processes. In: Reinhardt KA, Kern W (eds) *Handbook of silicon wafer cleaning technology*, 2nd edn. William Andrew, New York
- Gan W, Yang L, He Y, Zeng R, Cervera ML, de la Guardia M (2000) Mechanism of porous core electroosmotic pump flow injection system and its application to determination of chromium(VI) in waste-water. *Talanta* 51(4):667–675
- Herr AE, Molho JI, Santiago JG, Mungal MG, Kenny TW, Garguilo MG (2000) Electroosmotic capillary flow with nonuniform zeta potential. *Anal Chem* 72:1053–1057
- Hunter RJ (1981) *Zeta potential in colloidal science: principles and applications*. Academic Press, London
- Jiang LN, Mikkelsen J, Koo JM, Huber D, Yao SH, Zhang L, Zhou P, Maveety JG, Prasher R, Santiago JG, Kenny TW, Goodson KE (2002) Closed-loop electroosmotic microchannel cooling system for VLSI circuits. *IEEE Trans Compon Packag Technol* 25(3):347–355
- Jiménez ML, Arroyo FJ, Carrique F, Delgado AV (2007) Surface conductivity of colloidal particles: experimental assessment of its contributions. *J Colloid Interface Sci* 316:836–843
- Laser DJ, Santiago JG (2004) A review of micropumps. *J Micromech Microeng* 14(6):R35–R64
- Lazar LM, Karger BL (2002) Multiple open-channel electroosmotic pumping system for microfluidic sample handling. *Anal Chem* 74(24):6259–6268
- Liu SR, Dasgupta PK (1992) Flow-injection analysis in the capillary format using electroosmotic pumping. *Anal Chim Acta* 268(1):1–6
- Lyklema J, Minor M (1998) On surface conduction and its role in electrokinetics. *Colloids Surf A: Physicochem Eng Aspects* 140:33–41
- Mavré F, Robbyn KA, Laws DR, Chow KF, Chang BY, Crooks JA, Crooks RM (2010) Bipolar electrodes: a useful tool for concentration, separation, and detection of analytes in micro-electrochemical systems. *Anal Chem* 82:8766–8774
- Miao J, Xu Z, Zhang X, Wang N, Yang Z, Sheng P (2007) Micropumps based on the enhanced electroosmotic effect of aluminum oxide membranes. *Adv Mater* 19(23):4234–4237
- Paul PH, Arnold DW, Rakestraw DJ (1998) Electrokinetic generation of high pressures using porous microstructures. In: Harrison DJ, van den Berg A (eds) *Micro total analysis system*. Springer, New York, pp 49–52
- Prakash P, Grissom MD, Rahn CD, Zydney AL (2006) Development of an electroosmotic pump for high performance actuation. *J Membr Sci* 286(1–2):153–160

- Qian S, Duval JFL (2006) Coupling between electroosmotically driven flow and bipolar faradaic depolarization processes in electron-coupling microchannels. *J Colloid Interface Sci* 297:341–352
- Rashchi F, Xu Z, Finch JA (1998) Adsorption on silica in Pb- and Ca-SO₄-CO₃ systems. *Colloids Surf A: Physicochem Eng Aspects* 132(159):171
- Razunguzwa TT, Timperman AT (2004) Fabrication and characterization of a fritless microfabricated electroosmotic pump with reduced pH dependence. *Anal Chem* 76(5):1336–1341
- Reichmuth DS, Chirica GS, Kirby BJ (2003) Increasing the performance of high-pressure, high-efficiency electrokinetic micropumps using zwitterionic solute additives. *Sens Actuat B Chem* 92:37–43
- Rice CL, Whitehead R (1965) Electrokinetic flow in a narrow cylindrical capillary. *J Phys Chem* 69:4017
- Selvaganapathy P, Ki YSL, Renaud P, Mastrangelo CH (2002) Bubble-free electrokinetic pumping. *J Microelectromech Syst* 11(5):448–453
- Shin W, Lee JM, Nagarale RK, Shin SJ, Heller A (2011) A miniature, nongassing electroosmotic pump operating at 0.5 V. *J Am Chem Soc* 133:2374–2377
- Squires TM (2009) Induced-charge electrokinetics: fundamental challenges and opportunities. *Lab Chip* 9:2477–2483
- Tanaka N, Kobayashi H, Ishizuka N, Minakuchi H, Nakanishi K, Hosoya K, Ikegami T (2002) Monolithic silica columns for high-efficiency chromatographic separations. *J Chromatogr A* 965(1–2):35–49
- Toh GM, Corcoran RC, Dutta D (2010) Sodium silicate based sol-gel structures for generating pressure-driven flow in microfluidic channels. *J Chromatogr A* 1217:5004–5011
- Tripp JA, Svec F, Frechet JMJ, Zeng SL, Mikkelsen JC, Santiago JG (2004) High-pressure electroosmotic pumps based on porous polymer monoliths. *Sens Actuat B Chem* 99(1):66–73
- Vajandar SK, Xu D, Markov DA, Wikswo JP, Hofmeister W, Li D (2007) SiO₂-coated porous anodic alumina membranes for high flow rate electroosmotic pumping. *Nanotechnology* 18:275705
- Wallner JZ, Nagar N, Friedrich CR, Berstrom LP (2007) Macro porous silicon as pump media for electro-osmotic pumps. *Phys Stat Sol (a)* 204(5):1327–1331
- Wang XY, Cheng C, Wang SL, Liu SR (2009) Electroosmotic pumps and their applications in microfluidic systems. *Microfluid Nanofluidics* 6(2):145–162
- Wiza JL (1979) Microchannel plate detectors. *Nucl Instrum Methods* 162(1–3):587–601
- Xu Z, Miao J, Wang N, Wen W, Sheng P (2011) Digital flow control of electroosmotic pump: Onsager coefficients and interfacial parameter determination. *Solid State Commun* 151:440–445
- Yanagisawa N, Dutta D (2010) Pressure generation at the junction of two microchannels with different depths. *Electrophoresis* 31:2080–2088
- Yao S, Hertzog DE, Zeng S, Mikkelsen JC, Santiago JG (2003) Porous glass electroosmotic pumps: design and experiments. *J Colloid Interface Sci* 268(1):143–153
- Yao S, Myers AM, Posner JD, Rose KA, Santiago JG (2006) Electroosmotic pumps fabricated from porous silicon membranes. *J Microelectromech Syst* 15(3):717–728
- Zeng S, Chen CH, Mikkelsen JC, Santiago JG (2001) Fabrication and characterization of electroosmotic micropumps. *Sens Actuat B Chem* 79(2–3):107–114
- Zou HF, Huang XD, Ye ML, Luo QZ (2002) Monolithic stationary phases for liquid chromatography and capillary electrochromatography. *J Chromatogr A* 954(1):5–32